JOURNAL OF SPACECRAFT AND ROCKETS
Vol. 43, No. 6, November–December 2006

Analysis of Gossamer Structures Using Assumed-Strain Solid-Shell Finite Elements

Keejoo Lee* and Sung W. Lee†
University of Maryland, College Park, Maryland, 20742

DOI: 10.2514/1.19405

The objective of this study is to investigate the applicability of assumed-strain solid-shell finite elements for analysis of gossamer space and near-space structures such as solar sails and scientific balloons. The solid-shell element formulation that alleviates the element locking via the assumed-strain approach has been successfully used for analysis of extremely thin structures. In this study, quadruple precision is explored to further extend the capability of the nine-node assumed-strain solid-shell elements to analyses of extremely thin structures. As examples, geometrically nonlinear static analyses of solar sail ribbons and a square membrane are carried out, without using any stabilizing scheme. Subsequently, the assumed-strain solid-shell element formulation with quadruple precision are successfully used to determine the deformed shape and the stress distribution of a scientific balloon at various altitudes.

I. Introduction

AN increasing number of space and near-space applications require large area with lower mass, which renders extremely thin and highly flexible membrane structures an attractive option for construction of space systems components such as deep space antennas, Earth radiometers, radars, concentrators, telescopes, sunshield, solar sails, and solar arrays [1] and for construction of near-space surveillance and communication systems or advanced high-altitude platforms such as stratospheric airships and balloons [2]. For example, the gossamer space structures such as solar sails are expected to have dimensions that are several kilometers long, but only micrometers thick. Full-scale testing of gossamer space and near-space structures is difficult because of their large size and extreme flexibility, and the lack of zero gravity environments on the ground. Accordingly, it is likely that computational modeling techniques will play an increasingly important role for the analysis and simulation of large, ultralightweight space and near-space systems.

Despite efforts made in numerical analyses via the versatile finite element method, there remain many computationally challenging aspects. For example, gossamer structures are susceptible to structural wrinkling due to their very small bending stiffness. However, it is rather difficult to numerically predict the wrinkling amplitude. A geometrically nonlinear shell-based analysis has been used to predict the wrinkling amplitude as well as to account for both membrane and bending deformations [3–5]. Tessler et al. [5] used a commercial finite element code to simulate the formation of the wrinkling in thin-film membranes. In their study, quasi-static shell analyses of the membrane were conducted with a volume-proportional numerical damping scheme, provided in the commercial code, to avoid local instability. The resulting wrinkling pattern was also favorably compared with the experimental data. However, the proportional coefficient chosen to stabilize the local response was arbitrary.

Another example of computational challenges in analysis of gossamer space structures is to predict large deflection of solar sails with extremely low bending stiffness. Wang et al. [6] used stabilizing schemes to analyze a solar sail ribbon subjected to its own weight to demonstrate the need of the explicit time integration scheme. However, according to their study, this approach is computationally intensive due to small time step requirements for stability and accuracy.

Computational modeling of near-space structures such as scientific balloons is challenging due to their extreme flexibility and underconstrained nature [7,8]. For example, determination of balloon shapes and stress distributions at various altitudes is indispensable to ensuring structural integrity of the balloons. However, this seemingly simple problem turns out to be quite formidable because of numerical difficulties associated with highly thin-film material, the huge balloon size, and the underconstrained nature of the balloons.

To address these computationally challenging problems, one may consider using shell finite elements tailored specifically for analysis of gossamer space and near-space structures. In general, unless special care is taken, shell elements suffer from a numerical instability called element locking when their thickness becomes very small. Among various shell approaches, the assumed-strain formulation has been successfully used to alleviate the numerical instability in thin structures, in combination with the solid-shell approach. Lee and Lee [3] conducted a preliminary study on extending the use of assumed-strain solid-shell elements for analysis of extremely thin beams and plates via using quadruple precision. In their study, it was shown that the use of quadruple precision can help avoid numerical problems such as element locking beyond the range of thinness found in gossamer space and near-space structures.

In the present study, a more extensive investigation is carried out on the applicability of the assumed-strain solid-shell approach, combined with quadruple precision, to analysis of gossamer space and near-space structures. Initial tests are conducted on extremely thin beams and plates and circular rings. Subsequently, nine-node assumed-strain solid-shell elements with quadruple precision are used to model gossamer structures such as membranes and solar sail ribbons. Geometrically nonlinear static analyses of these gossamer space structures are conducted without any stabilizing schemes. Finally, techniques are introduced to determine configurations of a scientific balloon at various altitudes and corresponding stresses in the balloon envelope via geometrically nonlinear static analysis.

II. Assumed-Strain Solid-Shell Elements

An assumed-strain formulation is combined with a geometrically nonlinear solid-shell formulation that allows large displacement. The geometrically nonlinear formulation is based on the total Lagrangian description that employs Green's strain and the second

Presented as Paper 1802 at the 46th AIAA/ASME/ASCE/AHS/ASC Structures, Structural Dynamics and Materials Conference, Austin, TX, 18–21 April 2005; received 9 August 2005; accepted for publication 19 July 2006. Copyright © 2006 by the American Institute of Aeronautics and Astronautics, Inc. All rights reserved. Copies of this paper may be made for personal or internal use, on condition that the copier pay the $10.00 per-copy fee to the Copyright Clearance Center, Inc., 222 Rosewood Drive, Danvers, MA 01923; include the code $10.00 in correspondence with the CCC.

*Research Associate, Department of Aerospace Engineering, 3181 Glenn L. Martin Hall. Member AIAA.

†Professor, Department of Aerospace Engineering, 3181 Glenn L. Martin Hall. Member AIAA.

Piola–Kirchhoff stress tensors. The solid-shell approach treats the shell as a three-dimensional solid that allows transverse shear deformation as well as thickness change [9–11]. For the solid-shell elements, the description of the kinematics of deformation is based on vector variables, which enables large increments in geometrically nonlinear analyses. The high-order solid-shell elements (e.g., nine-node elements) have been often chosen for analysis of thin, curved structures due to their intrinsic curved nature in the description of geometry and kinematics of deformation, compared with the lower-order solid-shell elements (e.g., four-node elements). These solid-shell elements are susceptible to element locking when the thickness becomes very small. An assumed-strain formulation that introduces displacement-independent strain field within the element can be used to alleviate the element locking problem. The assumed-strain parameters are eliminated via satisfying compatibility equations between the displacement-dependent strain field and the displacement-independent strain field at the element level. A brief description of the assumed-strain solid-shell formulation is provided in this section.

A. Equilibrium and Compatibility Equations

For a solid in equilibrium, a virtual work form of equilibrium equations is expressed as follows:

$$\int_V \delta\bar{\boldsymbol{\varepsilon}}^T \boldsymbol{\sigma}\, \mathrm{d}V - \delta W = 0 \tag{1}$$

where $\delta\bar{\boldsymbol{\varepsilon}}$ is the virtual displacement-dependent strain vector, $\boldsymbol{\sigma}$ is the second Piola–Kirchhoff stress vector, δW is the virtual work due to the applied load and V is the volume of the undeformed configuration. In the assumed-strain formulation, in addition to the displacement-dependent strain vector $\bar{\boldsymbol{\varepsilon}}$, a displacement-independent strain vector $\boldsymbol{\varepsilon}$, assumed independently of $\bar{\boldsymbol{\varepsilon}}$, is introduced to alleviate element locking. The two strain vectors are related through the compatibility equation as

$$\int_V \delta\boldsymbol{\varepsilon}^T \boldsymbol{C}(\bar{\boldsymbol{\varepsilon}} - \boldsymbol{\varepsilon})\, \mathrm{d}V = 0 \tag{2}$$

where $\delta\boldsymbol{\varepsilon}$ is the virtual displacement-independent strain vector and $\boldsymbol{C}$ is the matrix of elastic stiffness constants [9–11]. The Piola–Kirchhoff stress vector $\boldsymbol{\sigma}$ is related to the independent strain vector $\boldsymbol{\varepsilon}$ such that

$$\boldsymbol{\sigma} = \boldsymbol{C}\boldsymbol{\varepsilon} \tag{3}$$

B. Finite Element Discretization

For geometrically nonlinear analyses, an incremental form of the preceding equilibrium and compatibility equations is used. The incremental form is obtained via plugging incremental expressions for stress and strain vectors into the equations.

For the assumed-strain formulation, the displacement-independent strain vector is defined within an element and expressed symbolically as

$$\boldsymbol{\varepsilon} = \boldsymbol{P}\boldsymbol{\alpha} \tag{4}$$

where $\boldsymbol{P}$ is a matrix of assumed-strain shape functions and $\boldsymbol{\alpha}$ is a column vector of assumed-strain parameters. Because the assumed-strain parameters are eliminated at element level, there is no increase in the number of unknowns at global level. A detailed description of the assumed-strain solid-shell element formulation is provided by Park et al. [10] for structures undergoing large static deformation.

Finite element discretization for the incremental forms of Eqs. (1) and (2), and assembly of all elements results in

$$\boldsymbol{K}\,\Delta\boldsymbol{q} = \Delta\boldsymbol{Q} \tag{5}$$

where $\boldsymbol{K}$ is the global tangent stiffness matrix, $\Delta\boldsymbol{q}$ is the global incremental nodal DOF vector, and $\Delta\boldsymbol{Q}$ is the global load vector due to equilibrium imbalance.

C. Arithmetic with Double and Quadruple Precision

The element locking problem has been successfully resolved via using the assumed-strain solid-shell formulation with double precision for thin structures with dimensions ranging from 10^2 to 10^3 in terms of length-to-thickness ratios. However, gossamer space structures such as solar sails may call for a membrane structure with a length of 10^2 m and a thickness of 10^{-7} m. This leads to the length-to-thickness ratio of 10^9, and the shell elements with double precision may not be adequate to overcome the numerical problems and fail to yield meaningful results when they are used to model these extremely thin membrane structures. Accordingly, one may extend the effective range of length-to-thickness ratios for the assumed-strain formulation solid-shell element via simply adopting the quadruple precision.

III. Locking Tests

The effect of element locking in analysis of extremely thin structures is investigated using two versions of nine-node assumed-strain solid-shell elements, one with double precision and the other with quadruple precision. The analysis is performed on a personal computer (Macintosh G5) that supports both double and quadruple precision arithmetic.

A. Beam Bending

To examine the effect of shear locking on the applicable limit of the solid-shell approach, a beam under a uniformly distributed load is considered. The boundary conditions are either clamped or simply supported. Because of symmetry in geometry and loading, one-half of the beam is modeled using 8×1 uniform meshes.

In Fig. 1, the maximum transverse displacement of the clamped beam, normalized to the exact solution based on the Bernoulli–Euler beam bending theory, is plotted with respect to the length-to-thickness (L/t) ratios. As observed in Fig. 1, the solid-shell elements with double precision are effective up to the length-to-thickness ratio of 10^5 for the clamped boundary conditions. The solution with double precision begins to rapidly deteriorate beyond $L/t = 10^6$ and does not converge even when the meshes are progressively refined. However, the effective range of length-to-thickness ratios for assumed-strain solid-shell elements can be significantly extended using quadruple precision. As shown in Fig. 1, the effectiveness of the solid-shell approach is extended to 10^{13}.

The effectiveness of the solid-shell approach is examined on a simply supported beam subjected to constant lateral pressure. In Fig. 2, the maximum transverse displacement of the simply supported beam, normalized to the exact solution based on the Bernoulli–Euler beam bending theory, is plotted with respect to the length-to-thickness ratio. As observed, the solid-shell elements with

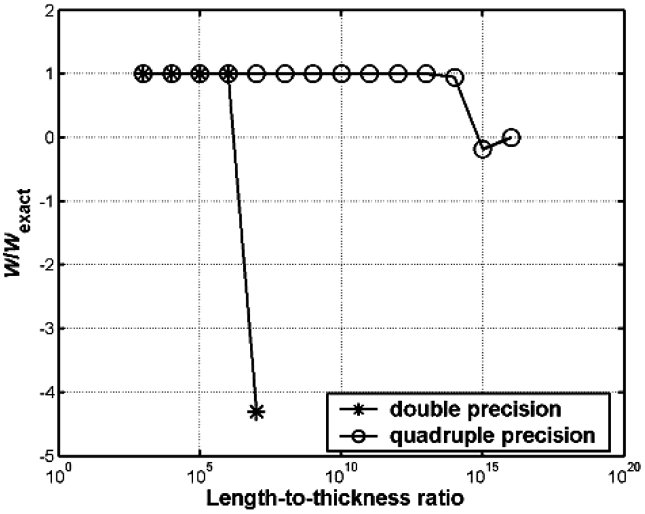

Fig. 1 w/w_{exact} **vs length-to-thickness-ratio (clamped beam).**

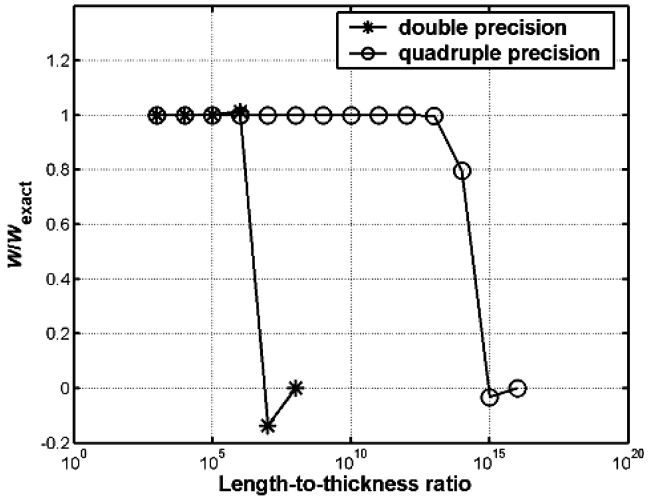

Fig. 2 w/w_{exact} vs length-to-thickness-ratios (simply supported beam).

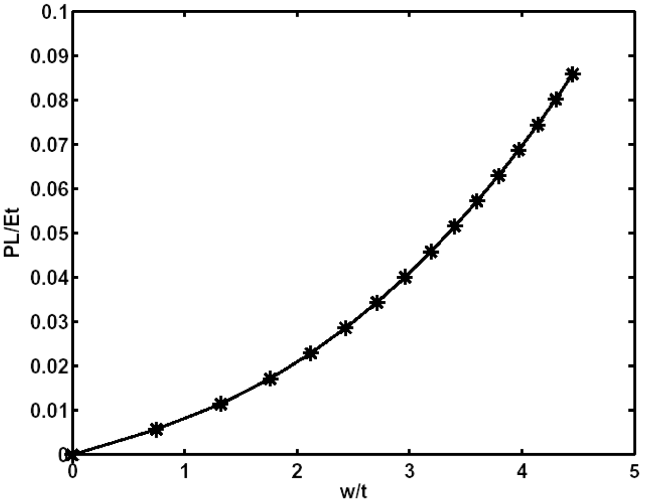

Fig. 4 Load vs w displacement-to-thickness.

double precision are effective up to a length-to-thickness ratio of 10^5 whereas the solid-shell elements with quadruple precision are effective up to a length-to-thickness ratio of 10^{13}. Irrespective of the boundary conditions, the modeling capabilities of solid-shell elements are significantly enhanced using quadruple precision.

B. Clamped Plate

For a numerical test, solid-shell elements with quadruple precision are used to model a clamped square plate under uniformly distributed loadings. Because of the symmetry in loading, geometry, and boundary conditions, only one-quarter of the plate is modeled using 4×4 meshes.

In Fig. 3, the out-of-plane displacement at the plate center, normalized to the analytical solution based on Kirchhoff theory is shown with respect to length-to-thickness ratio. With quadruple precision, solid-shell elements are able to perform effectively up to L/t of 10^{15}.

Another quadruple precision test is conducted on a plate undergoing geometrically nonlinear deflections under uniformly distributed loadings. The plate has a length-to-thickness ratio of 10^{15}. Figure 4 shows the maximum displacement W at the plate center, normalized to the thickness of the plate plotted against pressure P, normalized to a length-to thickness ratio. Calculations are carried out using a 4×4 mesh.

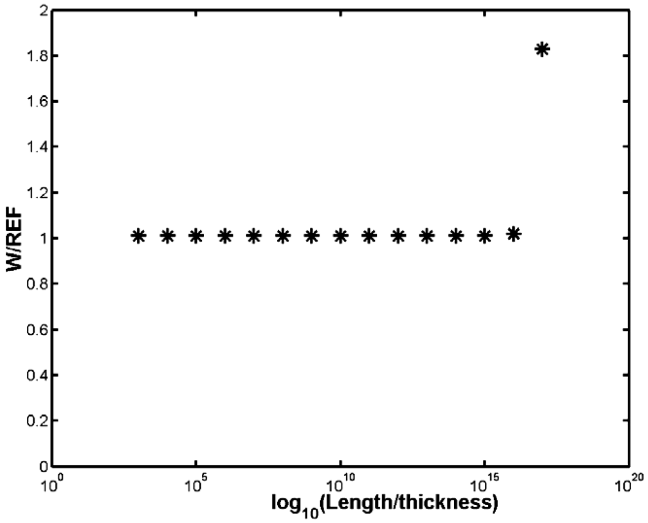

Fig. 3 w/w_{exact} vs length-to-thickness-ratio (quadruple precision).

C. Pinched Ring

For curved structures, the solid-shell elements suffer from membrane locking when their thickness is small compared to their radius. In this study, the effective range of radius-to-thickness ratio for the assumed-strain solid-shell elements is determined via using a numerical test on a pinched ring. A ring pinched at the top and bottom, as shown in Fig. 5, is considered. The radius and width of the ring are 100 m and 1 m, respectively. For material properties, Young's modulus is 1 GPa and Poisson's ratio is 0.0. Because of symmetry in loading and geometry, one-eighth of the ring is modeled using 8(circumferential) $\times$ 1(width) elements. Geometrically linear analyses are carried out for rings that have various thicknesses, and the resulting displacement w_A at point A in Fig. 5 is compared to the existing exact solution [12]. The exact solution is

$$w_A = 0.8927 \frac{P}{E} \left(\frac{R}{t}\right)^3 \tag{6}$$

where P is the magnitude of the concentrated force, E is Young's modulus, R is the radius, and t is the thickness.

As shown in Fig. 6, the effective range of the radius-to-thickness ratio is significantly extended using quadruple precision, from 10^4 to 10^{12}. Note that the effective radius-to-thickness ratio is even lower than the effective length-to-thickness ratio observed in the transverse shear locking tests.

IV. Analyses of Thin Ribbons

Thin solar sail ribbons under their own weight are chosen as an example. Wang et al. [6] conducted quasi-static analyses of a 100 m long ribbon via using ad hoc stabilizing schemes such as artificial pretension and volume-proportional artificial damping. They

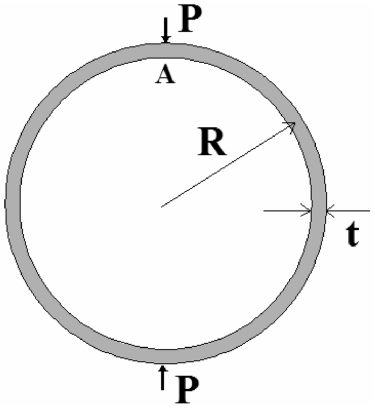

Fig. 5 A pinched ring.

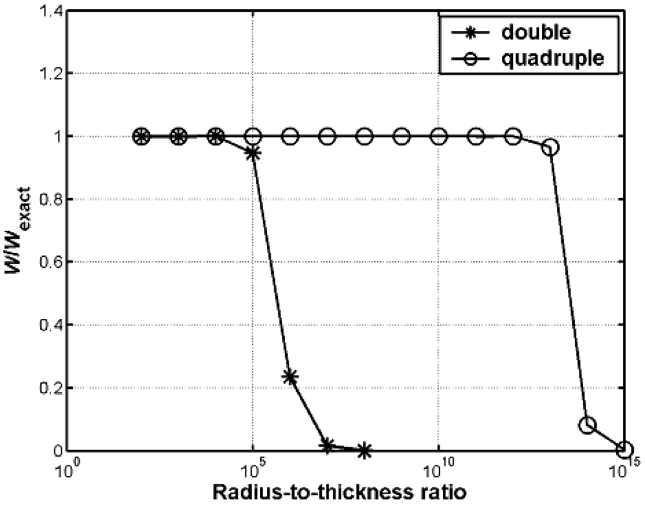

Fig. 6 w/w_{exact} vs radius-to-thickness ratios.

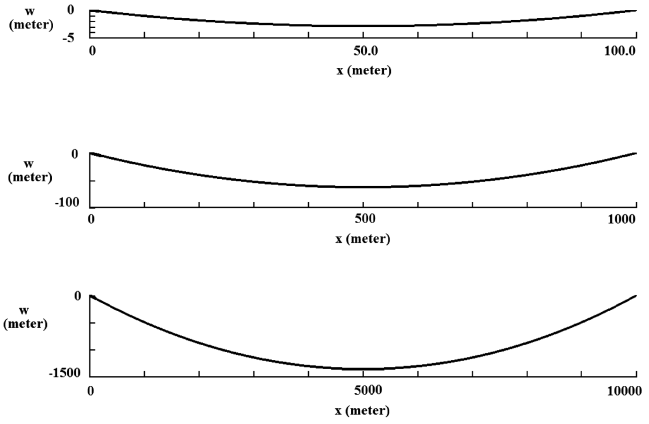

Fig. 7 Deflection (w) along the length direction (x) for the three ribbons (100 m, 1 km, 10 km long and 1 μm thick).

demonstrated that nonlinear static analyses based on double precision could encounter difficulties in convergence and accuracy. Subsequently, an explicit time integration scheme with the artificial damping was used to determine the transverse deflection of the thin ribbon.

In the present study, three solar sail ribbons with dimensions of 100 m, 1 km and 10 km long, 1 m wide and 1 μm thick are considered. The ribbons are pinned at both ends. The material is isotropic Kapton with a Young's modulus $E = 2.6$ GPa and a Poisson's ratio $\nu = 0.3$. The density is 1420 kg/m^3. One-half of the ribbon is modeled using ten elements in the length direction and two elements in the width direction due to symmetry in geometry and loading. Geometrically nonlinear static analyses are carried out using the nine-node assumed-strain solid-shell elements in conjunction with quadruple precision. No ad hoc stabilizing schemes such as artificial pretension and artificial damping are used. For thin ribbons with very small bending stiffness, applying the entire weight at the beginning of analysis results in very large deflection, causing convergence problems for subsequent iterations. Accordingly, a loading scheme that gradually increases its magnitude is introduced as follows: The weight of the ribbon is treated as transverse pressure, P expressed as

$$P = P_o \times 10^{-m} \tag{7}$$

where P_o is the target pressure or weight and 10^{-m} controls the magnitude of the applied pressure. In the present calculation, $m = 20, 15, 10, 5, 0$ are used successively over five load steps. This loading scheme allows the model to develop bending stiffness corresponding to the increased membrane stresses and enhances the convergence. The target pressure in Eq. (7) corresponding to gravity is expressed as

$$P_o = \rho g t \tag{8}$$

where ρ is the density, $g = 9.8$ m/s^2, and t is the ribbon thickness. The resulting maximum deflection of the ribbons is compared with an exact solution [13] expressed as

$$w_{\max} = -\left(\frac{3\rho g L^4}{64E}\right)^{1/3} \tag{9}$$

where L is the length of the ribbon. The resulting deflections at the center are very close to the exact solutions, irrespective of their length as shown in the Table 1.

Figure 7 shows the side views of deformed shapes for the three ribbons under their own weight. The proposed loading scheme is remarkably robust and produces the solution efficiently, irrespective of the length-to-thickness ratio.

V. Wrinkling Formation in a Square Membrane

In a previous study [3], numerical simulation to predict wrinkling formation in a flat square membrane subjected to two opposite corner point loads was conducted using a dynamic scheme that includes the effect of fictitious damping and uses geometrical imperfections in trigonometric form. However, the analyses were based on double-precision arithmetic, and the result was not properly validated due to lack of experimental data.

Recent studies [4,5] showed that wrinkling in a square membrane subjected to four corner loads can be captured via eliminating the sharp-corner meshes and introducing an initial out-of-plane deflection through buckling analysis or random imperfection. In their study, a stabilizing scheme was used to expedite numerical convergence in the geometrically nonlinear quasi-static analyses.

In this paper, geometrically nonlinear static analyses are conducted, without using any ad hoc schemes, to simulate wrinkling formation in a square solar sail membrane via using quadruple precision-based assumed-strain shell elements. The solar sail membrane, subjected to tensile loads (2.45 N) at four corners as shown in Fig. 8, is 0.5 m long, and is made of 2.54×10^{-5} m thick Kapton film. Material properties are identical to ones used for the previous ribbon examples. Because of symmetry in loading and geometry, one-eighth of the membrane is modeled using 6×20 elements. Two modeling techniques introduced by Tessler et al. [5] are adopted. Elimination of sharp corners is carried out, and the concentrated force is replaced by statically equivalent distributed force. Randomly generated out-of-plane imperfections are used, with various amplitudes in the corner regions alone. The resulting model with symmetry conditions is shown in Fig. 9. The resulting wrinkling pattern for the square membrane is shown in Fig. 10, where the four wrinkles across the loading corner regions are predicted. The amplitude of the wrinkling pattern ranges from -0.61 to 0.25 mm.

Table 1 Maximum deflection for the three ribbons

Ribbon length, m	Thickness, m	Mesh	Exact solution for $w_{\max}$, m	Numerical solution for $w_{\max}$, m
$L = 10^2$	$t = 10^{-6}$	10×2	-2.927	-2.927
$L = 10^3$	$t = 10^{-6}$	10×2	-6.307×10^1	-6.301×10^1
$L = 10^4$	$t = 10^{-6}$	10×2	-1.359×10^3	-1.354×10^3

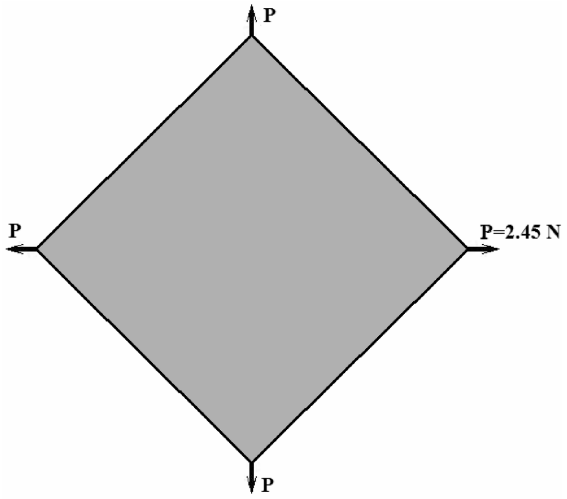

Fig. 8 A square Kapton membrane subjected to four corner loads ($P = 2.45$ N).

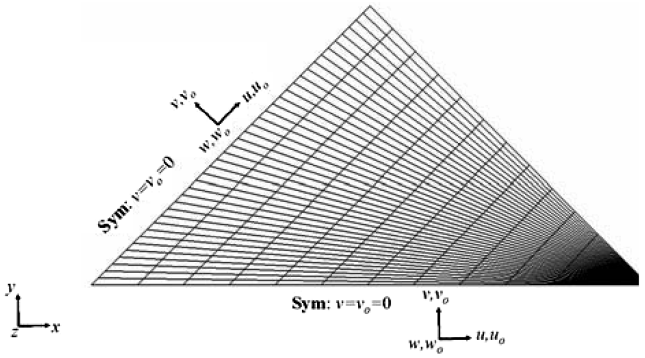

Fig. 9 One-eighth model of the square membrane with symmetry conditions (6 × 20 mesh).

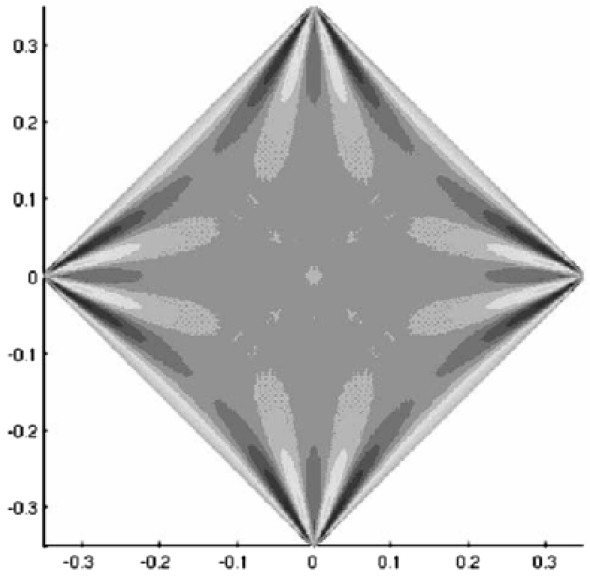

Fig. 10 Wrinkling pattern of the square Kapton membrane (0.5 m, $P = 2.45$ N).

VI. Analyses of Scientific Balloons

Scientific balloon envelopes are built via assembling hundreds of gores in the circumferential direction. A gore is a combination of two parts: load tape and skin. The load tape plays the role of carrying most of the load along the meridian direction. The skin, made of extremely thin-film material, contains helium gas inside the envelope and transfers the pressure differential across the balloon surface to the load-carrying tape. The balloon envelope formed by the multiple gores is joined to circular, rigid plates at the nadir and apex. The film material is extremely thin compared to other dimensions of the scientific balloons such as balloon height and radius. Computational modeling of scientific balloons is challenging mainly due to their extreme flexibility.

Scientific balloons go through large shape change as they ascend to the stratosphere. For example, the volume at launch is only a few percent of the fully deployed volume. In this paper, techniques are introduced to determine configurations of a scientific balloon at various altitudes and to compute corresponding stresses in the balloon envelope, via a geometrically nonlinear static analysis. The nine-node assumed-strain solid-shell elements with quadruple precision is selected to avoid the element locking problem as well as to properly represent the curved geometry and kinematics of deformation.

A. Balloon Design and Geometry

For zero-pressure scientific balloons, their gore shape is designed not to stress the skin material in the circumferential direction at the full deployment. Design parameters and mechanical properties of balloon materials are as follows:

Design altitude, km: 37.5
Design volume, MCM: 1.12
Number of gores: 172
Weight of payload, kN: 35.23
Density of film, kg/m^3: 1.805×10^3
Density of load tape, kg/m^3: 4.316×10^3
E of tape, GPa: 2.813
E of skin, GPa: 0.301
ν of skin: 0.83

The natural-shape equations [14] are used to find the float configuration via satisfying the force equilibrium between the total lift due to buoyancy and the gross weight. The geometry parameters (in meters) of the designed balloon are as follows:

Gore length: 201.35
Skin thickness: 2.0×10^{-5}
Film thickness: 5.1×10^{-5}
Film width: 5.1×10^{-2}
Radius at the apex: 0.53
Radius at the nadir: 0.078

Note that the ratio of the gore length to the skin thickness is about 10^7, which is beyond the limit of double-precision shell elements ($R/t = 10^4$). Indeed, initial attempts to analyze this example with double-precision arithmetic were unsuccessful.

B. Structural Modeling and Analysis of Balloons

The structural analysis of a scientific balloon is conducted under two primary premises. The balloon is rotationally symmetric throughout its deployment so that only one of the hundreds of gores is considered. The inertia effect is ignored due to the relatively benign acceleration. Whereas many structures are initially under the stress-free condition, this is not true for scientific balloons. A balloon structure cannot sustain its design shape unless properly loaded. For numerical analysis, the design shape at float is quite often the only shape available. Accordingly, the actual float configuration is determined via carrying out the analysis, using the design shape.

To represent the physical behavior of a scientific balloon, the vertical translation both at the nadir and the apex is allowed, as shown in Fig. 11. At the apex, the balloon is free to translate in the vertical direction whereas at the nadir, a fictitious spring is attached to the balloon to provide some translation in the vertical direction. The symmetry conditions are applied to the circumferential directions of the tape in one gore as shown in Fig. 11.

For the finite element modeling, the skin in a gore is modeled using one nine-node shell element in the circumferential direction and 40 elements in the meridian direction. For the two load tapes, each of them is modeled using a modified nine-node shell element under the

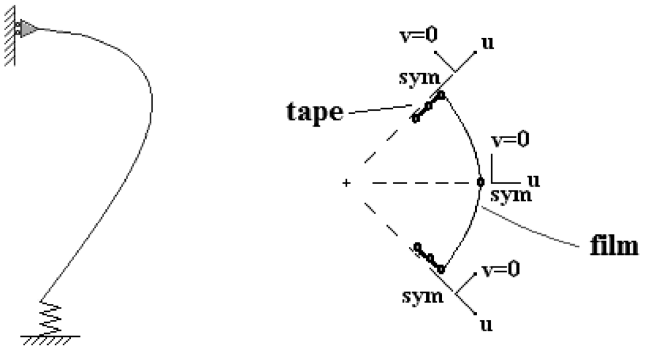

Fig. 11 Gore boundary conditions.

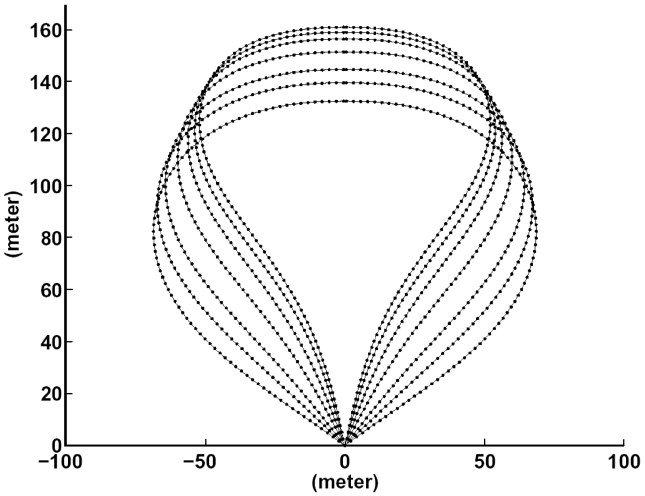

Fig. 12 Deformed configurations at various altitudes.

assumption that the three nodes in each cross-sectional plane in Fig. 11 are moving together, and 40 elements are used in the meridian direction. A fictitious spring is modeled using three continuous elements from the gore and one element in the meridian direction. For the skin element, it is assumed that films cannot sustain any compression in the circumferential direction.

Balloons use buoyancy to ascend. The lift of the balloon due to the buoyancy can be obtained via summing the pressure differential across the surface over the entire balloon. For balloon analyses, the pressure differential from the nadir to the apex is conventionally modeled as follows:

$$p = b(z - z_o) \tag{10}$$

where b is the buoyancy constant at an altitude and z_o is the zero-pressure height, where the pressure differential is equal to zero. The buoyancy constant is defined as multiplication of the difference between average densities of the gas and air to the acceleration constant due to gravity. The buoyancy constant is taken from the table of atmospheric properties and lifts of helium provided by Warren et al. [15]. An ascending balloon undergoes large deformation under the pressure differential loading over the balloon surface. The magnitude and direction of such loading is dependent on the deformed configuration. This interdependency of the pressure loading and the balloon shape is critical in the physical understanding of balloons. Accordingly, the shape and the pressure loading must be simultaneously determined in a repetitive manner until the next analysis produces the same shape and loading condition. In addition to the pressure loading, there exist a concentrated force of payload at the nadir and the distributed weight of the materials. Note that the weight distribution of materials is also dependent on the deformation.

Starting from the configuration at the float state (37.5 km), the geometrically nonlinear static analysis continues to the lower altitudes, and the resulting balloon configurations at various altitudes

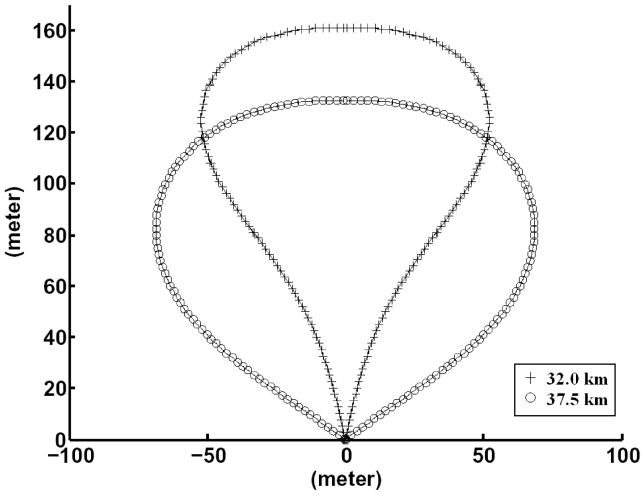

Fig. 13 Deformed configurations at float altitude (37.5 km) and 32.0 km.

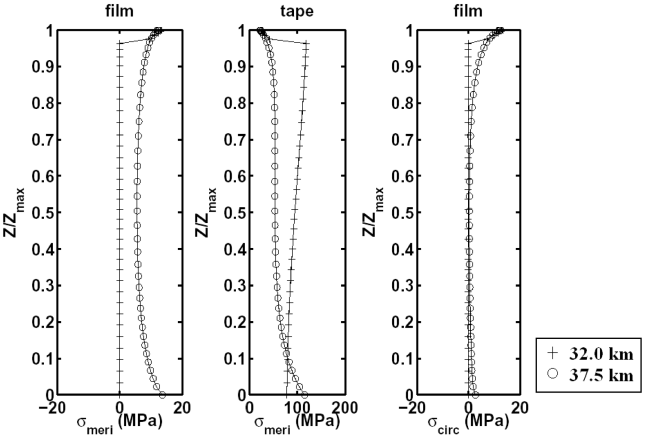

Fig. 14 Stress distributions at 37.5 km (float) and at 32.0 km (ascending).

are shown in Fig. 12. Profiles of the balloon at two altitudes are shown in Fig. 13.

Meridian stresses of the film along the nondimensional height for the two altitudes in Fig. 13 are shown in the left-most plot of Fig. 14. As observed, most of the film is free of the meridian stress before the full deployment. Approaching the float condition, the meridian stress of the film increases over the balloon envelope, and the circumferential stress, as shown in the right-most plot, slightly increases as well. This is consistent with the reduced tape stress in the meridian direction as shown in the middle plot.

VII. Conclusion

Numerical tests on the applicability of the nine-node assumed-strain solid-shell elements for analysis of extremely thin beams, plates, and rings were conducted using double- and quadruple-precision arithmetic. The results demonstrate that by using the quadruple precision, one can significantly extend the effective range of length-to-thickness or radius-to-thickness ratio for the assumed-strain solid-shell elements.

Subsequently, the assumed-strain solid-shell element formulation with quadruple precision was successfully used for analysis of example problems representative of gossamer space and near-space structures. Geometrically nonlinear static analyses of solar sail ribbons were carried out without using any ad hoc schemes to stabilize finite element models. Deformed shapes under own weight are determined via using a loading scheme that takes advantage of quadruple precision. The proposed loading scheme is robust and can be applied to bending analysis of extremely thin structures. For a

square membrane subjected to four corner loads, a wrinkling pattern is captured via conducting geometrically nonlinear static analysis without using other stabilizing schemes. The observed wrinkling pattern in the square membrane is qualitatively validated. Accordingly, there is a need for quantitative validation and further investigation on the wrinkling pattern in the membrane. Techniques are developed to determine the deformed shape of a scientific balloon at various altitudes during the ascent and the stress distribution for the skin and load tape materials at the corresponding altitudes.

The present study demonstrates that the finite element method based on the assumed-strain solid-shell formulation combined with quadruple precision arithmetic provides a computationally effective tool for analyses of gossamer space and near-space structures without using the ad hoc stabilizing schemes. This enhanced computational capability can help explore in detail the physics of gossamer structure in the future study.

Acknowledgment

The authors thank Gregory Clarke at NASA Goddard Space Flight Center for providing the geometry and material data for the scientific balloon.

References

[1] Jenkins, C. H. M., *Gossamer Spacecraft: Membrane and Inflatable Structures Technology for Space Applications*, Vol. 191, Progress in Astronautics and Aeronautics, AIAA, Reston, VA, 2000.

[2] Stewart, M. A., Frisbie, K., and Trinkle, G., "High-Altitude Surveillance," *GeoIntelligence*, July–Aug. 2004, pp. 28–33.

[3] Lee, K., and Lee, S. W., "Analysis of Gossamer Space Structures Using Assumed Strain Formulation Solid Shell Elements," AIAA Paper 2002-1559, 2002.

[4] Wong, Y. W., and Pellegrino, S., "Computation of Wrinkle Amplitudes in Thin Membranes," AIAA Paper 2002-1369, 2002.

[5] Tessler, A., Sleight, D. W., and Wang, J. T., "Nonlinear Shell Modeling of Thin Membranes with Emphasis on Structural Wrinkling," AIAA Paper 2003-1931, 2003.

[6] Wang, J. T., Chen, T., Sleight, D. W., and Tessler, A., "Simulating Nonlinear Deformation of Solar Sail Membranes Using Explicit Time Integration," AIAA Paper 2004-1580, 2004.

[7] Schur, W. W., "Structural Analyses of Balloons Employing Various Techniques to Overcome Difficulties Posed by the Underconstrained Nature of These Systems," AIAA Paper 96-0577, Jan 1996.

[8] Baginski, F. E., and Schur, W. W., "Structural Analysis of Pneumatic Envelopes: Variational Formulation and Optimization-Based Solution Process," *AIAA Journal*, Vol. 42, No. 2, 2003, pp. 304–311.

[9] Kim, Y. H., and Lee, S. W., "A Solid Element Formulation for Large Deflection Analysis of Composite Shell Structures," *Computers and Structures*, Vol. 30, Nos. 1–2, 1988, pp. 269–274.

[10] Park, H. C., Cho, C., and Lee, S. W., "Efficient Assumed Strain Element Model with Six DOF per Node for Geometrically Non-Linear Shells," *International Journal for Numerical Methods in Engineering*, Vol. 38, No. 24, 1995, pp. 4101–4122.

[11] Park, H. C., and Lee, S. W., "Local Coordinate System for Assumed Strain Shell Element Formulation," *Computational Mechanics Advances*, Vol. 15, No. 5, 1995, pp. 473–484.

[12] Cho, C., "An Improved Assumed Strain Shell Element Formulation Including Bubble Function Displacements," Ph.D. dissertation, Univ. of Maryland College Park, MD, 1996.

[13] Roark, R. J., and Young, W. C., *Formula for Stress and Strain*, McGraw–Hill, New York, 1975.

[14] Smalley, J. H., "Balloon Design Considerations," Scientific Ballooning Handbook, NCAR Technical Note NCAR-TN/LA-99, May 1975.

[15] Warren, J. C., Smalley, J. H., and Morris, A. L., *Aerostatic Lift of Helium and Hydrogen in the Atmosphere*, National Center for Atmospheric Research Technical Notes, Boulder, CO, Dec. 1971.

G. Agnes
Associate Editor